Computational Investigation into Pressure and Viscous Resistances of a Catamaran in Calm Water

Ahmad Fitriadhy[1,*], Nur Amira Adam[2], Buana Ma'ruf[3], Mohd Sofiyan Sulaiman[4], Faisal Mahmuddin[5]

[1] Program of Naval Architecture, Faculty of Ocean Engineering Technology and Informatics, Universiti Malaysia Terengganu, Kuala Terengganu, Terengganu, Malaysia
[2] School of Port, Logistics and Management, Netherlands Maritime University College, Johor, Malaysia
[3] Research Center for Hydrodynamics Technology, The National Research, and Innovation Agency (BRIN), Indonesia
[4] Program of Environmental Technology, Faculty of Ocean Engineering Technology and Informatics, Universiti Malaysia Terengganu, Kuala Terengganu, Terengganu, Malaysia
[5] Department of Marine Engineering, Engineering Faculty, Hasanuddin University, Makassar, Indonesia

ARTICLE INFO

ABSTRACT

The presence of incident divergent waves between two demi-hulls on catamaran ship will attempt to generate a non-linear hydrodynamic behaviour, which inherently induced an accuracy of predicting her total resistance (R_T). Correspondingly, this becomes an attractive factor to propose a more reliable prediction of the total ship's resistance through quantifying both of pressure and viscous resistances components. This paper presents computational investigation into predicting the viscous (C_V) and pressure coefficients (C_P) in calm water condition; whilst the rationale behind the analysis results explained. Several parameters have been taken into accounts in the computational simulation such as the effect of lateral separation (S/L) and longitudinal staggered (R/L) ratios at various Froude numbers. The preliminary validation shows that the total ship's resistance at various S/L and R/L ratios constitute a fairly good agreement as compared to the experimental results. In addition, the CFD simulations revealed that the highest C_V and C_P occurred at the Fr= 0.47. The comparison in various lateral separation ratio showed that the symmetrical catamaran produced highest C_V and C_P at S/L=0.2 and S/L=0.4, respectively. Meanwhile, the staggered catamaran with S/L=0.2 produces highest the values of C_V and C_P at R/L=0.4 and R/L = 0.2, respectively. It is merely concluded that the current computational prediction provides useful outcomes particularly to estimate the effective power at preliminary design stage.

1. Introduction

Design of a high-speed multihull vessel with less ship's resistance has been at the forefront among naval architecture research interest Insel *et al.,* [1], Seif *et al.,* [2]. Several hull form configurations of the multihull ships have been accordingly developed to investigate some proper criteria with respect to the geo-metrical configurations associated with the ship's speed. In case of

---

* *Corresponding author.*
E-mail address: naoe.afit@gmail.com (Ahmad Fitriadhy)

the catamaran ship, a complex fluid flow phenomenon between the demi-hull has become an attractive factor to be investigated, which may lead to the total ship's resistance performance.

The presence of simultaneous wave-fields interactions between two demi hulls on the catamaran is generally a highly complex phenomenon and superposed non-linearly to induce the total ship's resistance. This means that the resistance behaviour of the catamaran is obviously different as compared to the typical monohull ships, which could be easily defined using the mathematical approach Peng [3]. Initially, the theoretical approach has been proposed to predict the total ship's resistances of the catamaran ship due to flexibility to cope with a variety of problems, yet easy to do with a minimum cost. Besides, an experimental method is also carried out at towing tank to obtain more valid results involving the effect of the lateral separation between two demi-hull Jamaluddin *et al.*, [4], Molland *et al.*, [5,6], Brogolia *et al.*, [7] and Zaghi *et al.*, [8]. In particular, the investigation of interference effect of the resistance components such as wave resistance and viscous resistance in wide range of Froude number was conducted by Insel *et al.*, [1]. However, this physical model test was proven to be very impractical, costly and time-consuming. Hence, this situation creates a need for alternative solution method called as Computational Fluid Dynamic (CFD) approach, which is capable of producing reliable prediction to compensate inaccuracy and complex procedure from the theoretical and experimental model test, respectively Brogolia *et al.*, [9], Haase *et al.*, [10], He *et al.*, [11] and Zaghi *et al.*, [12]. In general, this computational approach has good agreement with the experimental model test at the towing-tank Wei He *et al.*, [11], Sadeghi and Hajivand [13] and Sadeghi and Zeraatgar [14].

This paper presents a computational investigation into pressure and viscous resistances of a catamaran in calm water as the extension work from Fitriadhy *et al.*, [15]. Here, a commercial CFD software, namely Numeca Fine^{TM}/Marine. was utilized by applying the incompressible unsteady Reynolds-Averaged Navier Stokes equations (RANS) is used in which RANSE and continuity equations are discretized by the finite volume method based on Volume of Fluid (VOF) to deal with the nonlinear free surface Adam *et al.*, [16], Fitriadhy *et al.*, [17], Fitriadhy *et al.*, [18], Fitriadhy *et al.*, [19]. Correspondingly, several parameters have been such as various lateral separation (S/L) and longitudinal staggered (R/L) ratios in the range of Froude number from Fr=0.19 to 0.66 have been taken into account in the computational simulations. Here, we have conducted experimental model tests as the preliminary validation of our computational setting, where the very confident and reliable computational results achieved in the total ship's resistance prediction paved the way for foreseeing the pressure and viscous resistance. The results are then comprehensively discussed through quantifying the total ship's resistance (R_T) into two resistance components such as pressure (R_P) and viscous (R_V) resistances. The reason behind this computational approach in then explained by representing the wave elevation, hydrodynamic pressure and turbulent viscosity surrounding the catamaran hull form.

2. Methodology
2.1 Governing Equation

The CFD flow solver on Numeca Fine^{TM}/Marine is based on the incompressible unsteady RANSE in which the solver applies the Finite Volume Method to build the spatial discretization of the transport equations. In addition, the velocity field is obtained from the momentum equations and the pressure field is extracted from the mass conservation constraint, or continuity equation, transformed into a pressure equation. In the case of turbulent flows, additional transport equations for modelled variables are solved in a form similar to that of the momentum equations and they can be discretized and solved using the same principles.

2.2 Conservation Equations

The flow solver can deal with multi-phase flows and moving grids. In the multi-phase continuum, considering incompressible flow of viscous fluid under isothermal conditions, mass, momentum and volume fraction conservation equations can be expressed as (using the generalized form of Gauss' theorem):

$$\frac{\partial}{\partial_t} \int_V p dV + \int_S \rho \left(\vec{U} - \overrightarrow{U_d}\right).\vec{n}\, dS = 0 \tag{1}$$

$$\frac{\partial}{\partial_t} \int_V \rho U_i dV + \int_S \rho U_i \left(\vec{U} - \overrightarrow{U_d}\right).\vec{n}\, dS = \int_S \left(\tau_{ij} I_j - p I_i\right).\vec{n}\, dS \\ + \int_V \rho g_i dV \tag{2}$$

$$\frac{\partial}{\partial_t} \int_V c_i dV + \int_S c_i \left(\vec{U} - \overrightarrow{U_d}\right).\vec{n}\, dS = 0 \tag{3}$$

where V is the control volume, bounded by the closed surface S with a unit normal vector $\vec{n}$ directed outward that moves at the velocity $\overrightarrow{Ud}$ with a unit normal vector $\vec{n}$. The notation of $\vec{U}$ and p represent the velocity and pressure fields, respectively. τ_i and g_i define the components of the viscous stress tensor and the gravity vector, respectively; whereas I_i is a vector whose components vanish, except for the component j which is equal to unity. c_i is the ith volume fraction for fluid i and is used to distinguish the presence (c_i=1) or the absence (c_i = 0) of ith fluid. Since a volume fraction between 0 and 1 indicates the presence of a mixture, the value of 1/2 is selected as a definition of the interface.

2.3 Turbulence Model

In the case of a basic computation for turbulent condition, we propose the SST k-ω (SST for shear-stress transport) model, which is available inside ISIS-CFD solver code, where k is the turbulent kinetic energy and ω is the specific dissipation rate. Menter [20,21], Menter [22,23] reported that the SST k-ω model combines several desirable elements of existing two-equation models. The two major features of this model are a zonal blending of model coefficients and a limitation on the growth of the eddy viscosity in rapidly strained flows. The zonal modelling uses Wilcox's k-ω model near solid walls and the standard k-ε model, in a k-ω formulation, near boundary layer edges and in free-shear layers. Spalart *et al.,* [24], Baldwin *et al.,* [25] highlighted that the SST k-ω model here is set to improve the predictions obtained with algebraic mixing-length models to develop a local model for complex flows, and to provide a simpler alternative to two-equation turbulence models. This means that this turbulent model improves the prediction of flows with strong adverse pressure gradients and separation.

The two transport equations of the model are defined below with a blending function F₁ for the model coefficients of the original ω and ε model equations and written as:

$$\frac{\partial \rho K}{\partial t} + \frac{\partial}{\partial x_j}\left(\rho U_j K - (\mu + \sigma_k \mu_t)\frac{\partial K}{\partial x_j}\right) = \tau_{tij}S_{ij} - \beta^* \rho \omega K \tag{4}$$

$$\frac{\partial \rho \omega}{\partial t} + \frac{\partial}{\partial x_j}\left(\rho U_j \omega - (\mu + \sigma_\omega \mu_t)\frac{\partial \omega}{\partial x_j}\right) = P_\omega - \beta \rho \omega^2$$
$$+ 2(1 - F_1)\frac{\rho \sigma_{\omega 2}}{\omega}\frac{\partial K}{\partial x_j}\frac{\partial \omega}{\partial x_j} \tag{5}$$

where the last source term of Eq. (5) represents the cross-diffusion term that appears in the transformed ω-equation from the original ε-equation. Menter *et al.,* [26] noted that the production term of ω is sometimes approximated as proportional to the absolute value of vorticity:

$$P_\omega \equiv 2\gamma\rho\left(S_{ij} - \frac{\omega S_{nn}\delta_{ij}}{3}\right)S_{ij} \cong \gamma\rho\Omega^2 \tag{6}$$

The auxiliary blending function F_1, designed to blend the model coefficients of the original k-ω model in boundary layer zones with the transformed k-ε model in free-shear layer and free-stream zones, is defined as follows:

$$F_1 = \tanh\left(\left[\min\left\{max\left\{\frac{\sqrt{K}}{0.09d\omega}, \frac{500\mu}{pd^2\omega}\right\}, \frac{4\emptyset\sigma_{\omega 2}k}{CD_{k\omega}d^2}\right\}\right]^4\right) \tag{7}$$

Where;

$$CD_{k\omega} = max\left\{\frac{2\rho\sigma_{\omega 2}}{\omega}\frac{\partial K}{\partial x_j}\frac{\partial \omega}{\partial x_j}, 10^{-20}\right\} \tag{8}$$

Here, $CD_{k\omega}$ is the cross-diffusion in the k-ω model.

It should be noted here that when calculating turbulence quantities, it is important to consider an appropriate cell meshing size. This can be explained by the fact that during computations using the Navier-Stokes equations the boundary layer near a solid wall contains high gradients. To properly capture it a sufficient number of grid points inside the boundary layer is essential. Here, an appropriate estimation of the cell meshing size y_{wall} for Navier-Stokes simulations including turbulence depends on the local Reynolds number, which is computed based on the wall variable y^+. This y^+ is a dimensionless parameter representing local Reynolds number in the near wall region. Referring to Manual Fine marine [27], the value of y^+ value associated with the first node near the wall will be referred to as y_1^+, where the equation of y_1^+ can be written as:

$$y_1^+ = \frac{\rho u_\tau y_{wall}}{\mu}$$

$$u_\tau = \sqrt{\frac{\tau_{wall}}{\rho}} = \sqrt{\frac{1}{2}\rho(V_{ref})^2 C_f} \tag{9}$$

where u_τ is the friction velocity. It is clear that the value of y_{wall} depends on the value of y_1^+. In addition, the estimation for y_{wall} as a function of a desired y_1^+, value is obtained using a truncated series solution of the Blasius equation as written in Eq. (10) below.

$$y_{wall} = 6 \left(V_{ref}/v\right)^{-7/8} \left(L_{ref}/2\right)^{1/8} y_1{}^+ \tag{10}$$

Note that the reference velocity, V_{ref}, can be taken from the body velocity. The reference length, L_{ref}, should be based on the body length since an estimation of the boundary layer thickness is implied in this calculation. For instance, in the case of a marine simulation, one could use the boat length, or the so-called length between perpendiculars, as reference length. This refers to the length of a vessel along the waterline from the forward surface of the stem, or main bow perpendicular member, to the after surface of the sternpost, or main stern perpendicular member. This is approximate, of course, as the thickness of the boundary layer will vary widely within the computational domain. Fortunately, it is only necessary to place y_1^+ within a range and not at a specific value.

2.4 Total Resistance Prediction of a Ship

Based on the traditional resistance theory, the total resistance of a ship can be expressed in Eq. (10) as the sum of the frictional resistance (R_F) and the residual resistance or called here as the pressure resistance (R_P).

$$R_T = R_F + R_V \tag{11}$$

where the coefficient of the total resistance is expressed as:

$$C_T = \frac{R_T}{0.5 \times \rho \times WSA \times V_s{}^2} \tag{12}$$

where R_T is the dimensional total resistance, ρ is the water density, WSA is the wetted surface area of the ship at rest and V_s is the forward ship's speed Kim *et al.*, [28].

3. Simulation Condition
3.1 Principal Data of Ship

The dimension of the rounded catamaran which is comprised of two demi-hull is presented in Table 1.

Table 1
Principal Dimensions of Catamaran

Description	Demi-hull	Catamaran
Length between perpendicular, *LBP* (m)	1.372	1.372
Breadth *b*, (m)	0.123	0.123
Draft *T*, (m)	0.078	0.078
Wetted Surface Area, *WSA (m²)*	0.2559	0.512
Volume of displacement, *V* (m³)	0.0072	0.0144
Displacement, Δ *(tonnes)*	7.222	14.444
Center of buoyancy, *KB (m)*	0.049	0.049

3.2 Simulation Parameters

Figure 1 shows several effects of S/L (the lateral separation ratio between two centrelines of the demi-hull) and R/L (represents the longitudinal staggered position ratio with respect to the demi-hull transom) at a wide range of Froude numbers (Fr).
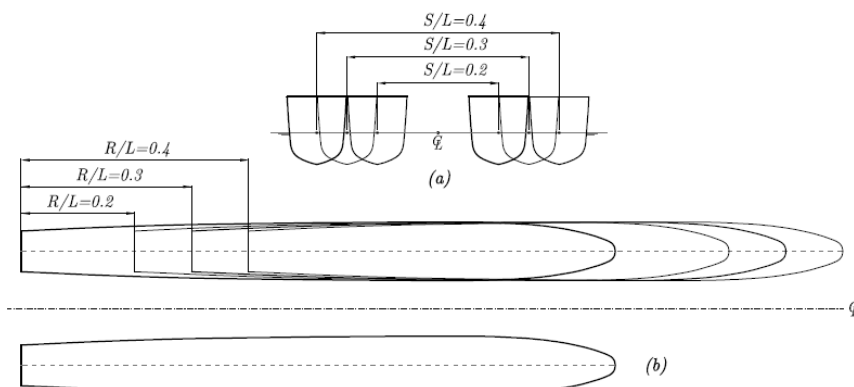
Fig. 1. Simulation Conditions on Predicting Total Resistances on the Catamaran due to: (a) Effect of S/L/ and (b) Effect of R/L

Correspondingly, the details of the simulation parameter for predicting the total resistance with regards to various configurations of the symmetrical and the staggered catamaran are summarized in Table 2.

Table 2
Matrix simulation of computational fluid dynamics for various S/L ratio, R/L ratio and Froude number

Matrix of CFD simulation		R/L				Froude number
		0.0	0.2	0.3	0.4	Fr
S/L	0.2	√	√	√	√	0.19, 0.28, 0.37, 0.56 and 0.66
	0.3	√	-	-	-	0.19, 0.28, 0.37, 0.56 and 0.66
	0.4	√	√	√	√	0.19, 0.28, 0.37, 0.56 and 0.66

For the validation purposes of computational models, the experimental model test has been conducted at towing-tank of Indonesian Hydrodynamic Laboratory (IHL) as seen in Figure 2.
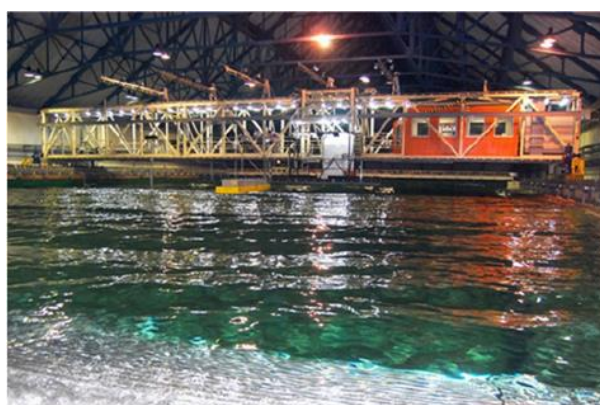
Fig. 2. Experimental Model Test at Towing-Tank Indonesia Hydrodynamic Laboratory

3.2.1 Computational domain and meshing generation

The unstructured hexahedral meshes have been used in the catamaran model as shown in Figure 3.
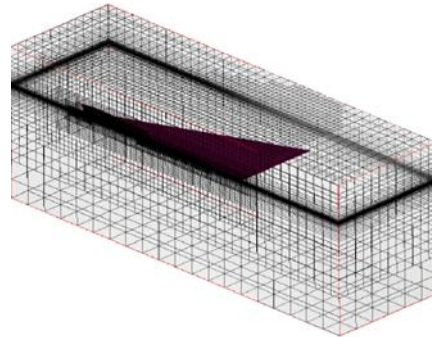
Fig. 3. Boundary Condition of Catamaran
Model

The local mesh refinement is added into the catamaran hull to improve mesh quality of the geometrical model. The detailed domains of this computational simulations are completely summarized in Table 3. Two different model settings have been applied

   i.   the symmetrical computational domain for the demi-hull and the symmetrical catamaran
        model
   ii. the fully computational domain for the staggered catamaran model.

Table 3
Computational Domain and Boundary Setting Conditions

Description	Distance From COG	Type	Condition
X_{min} (inlet)	1.0 L_{mh}	EXT	Far field
X_{max} (outlet)	3.0 L_{mh}	EXT	Far field
Y_{min} (side)	1.5 L_{mh}	MIR/EXT	Mirror/Far field
Y_{max} (side)	1.5 L_{mh}	EXT	Far field
Z_{min} (bottom)	1.5 L_{mh}	EXT	Prescribed pressure
Z_{max} (top)	0.5 L_{mh}	EXT	Prescribed pressure

The meshing generation of the catamaran model was created in HEXPRESS 3.1-1 software. It should be noted that an adequate number of mesh is very important towards accuracy and steadiness in the computational simulations. Hence, a mesh independent study may need to be performed for each of the four different initial numbers of the cell meshing, Table 4.

Table 4
Mesh Independent Study on Symmetrical Catamaran

Case	Number of Division Axis (X,Y,Z)	Initial No. of Cell Meshing	Total No. of Cell Meshing	R_T (N)
A	10×3×4	120	542,448	0.9198
B	15×5×6	450	1,568,833	0.9074
C	20×6×8	960	2,284,082	0.8914
D	40×12×16	7,680	5,273,144	0.8912

Initially, the cell meshing of 960 has been selected in all computational simulations of the symmetrical catamaran model with reasonable accuracy of the CFD solution. This can be explained by the fact that the increase of initial cell meshing up to 7,680 was unnecessary due to its insignificant influence into the computational results of the total resistance. Here, convergence of the solution is assessed by monitoring the residuals of continuity, velocity, and total resistance force (see Figure 4).
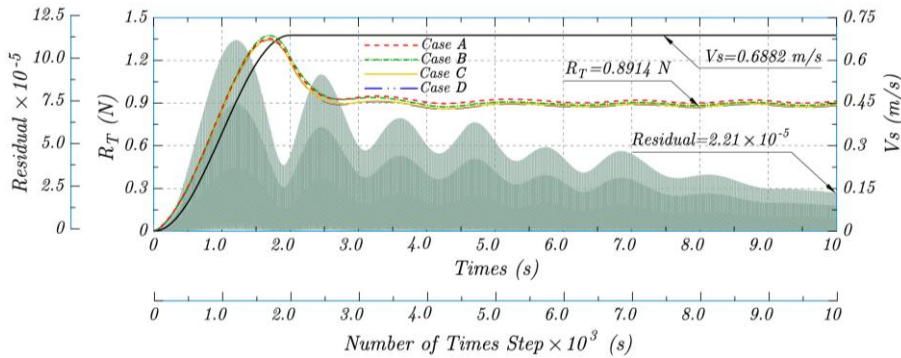
Fig. 4. Time-History for Residual Convergence of CFD Simulation (Symmetrical Catamaran, S/L=0.2 and Fr=0.19)

It should be noted that the residual convergence criterion is taken as $2.21e^{-05}$. Using a similar way, the optimum computational mesh numbers for the demi-hull and the staggered catamaran models have been suitably established (see Table 5).

Table 5
Selection of Computational Mesh Numbers

Model	Number of Division Axis (X,Y,Z)	Initial No. of Cell Meshing	Total No. of Cell Meshing
Demi-hull	20×6×8	960	1,668,271
Staggered Catamaran	20×12×8	1,920	4,157,533

Finally, a package software of CFView was used to visualize the wave pattern/free surface elevation, hydrodynamic pressure and turbulent viscosity for all various configurations of the symmetrical and the staggered catamaran as displayed in Figure 5.
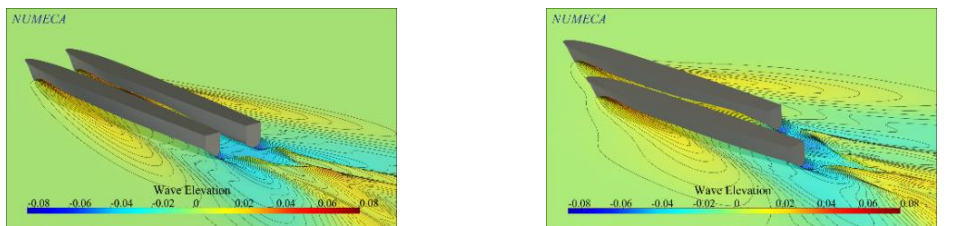
(a) Symmetrical Model (S/L=0.2) (b) Staggered Model $_{S/L}$=0.2 and $_{R/L}$=0.2)
Fig. 5. Example CFD Visualization of 3D-Wave Elevation (Fr=0.66)

4. Results and Discussion

The computational simulations of the total ship's resistance of the symmetrical and staggered catamaran model have been evaluated through quantifying the pressure and the viscous resistances. In general, the subsequent increase of the Froude numbers is proportional with the total ship's resistance for any configurations of the symmetrical and staggered catamaran models as displayed

in Figures 6, 7 and 8. Inversely. In particular, the total ship's resistance reaches the maximum value of C_T at the Froude number Fr=0.47 regardless of the symmetrical and staggered catamaran configurations; the further increase of the Froude number up to Fr=0.66 leads to reduce the value of C_T.
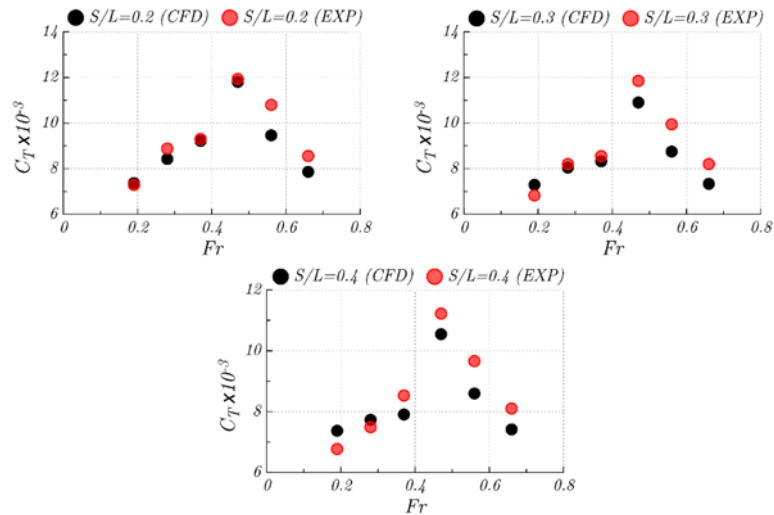
Fig. 6. Total Resistance Coefficients at Various S/L Ratios (R/L = 0)
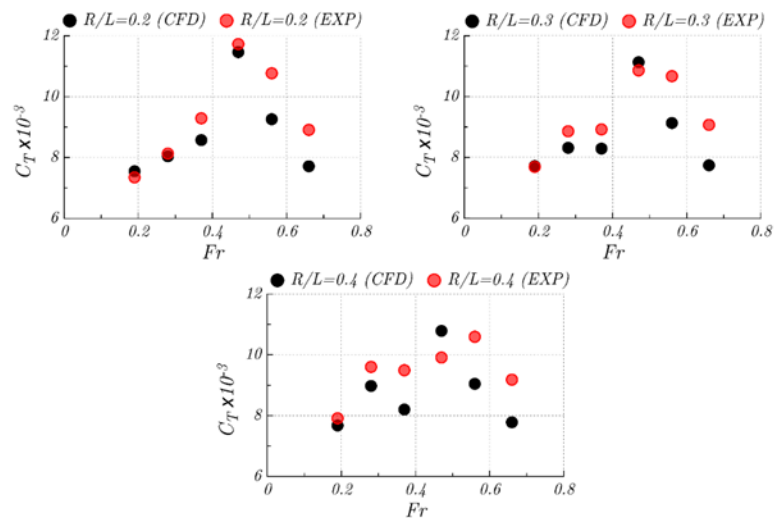
Fig. 7. Total Resistance Coefficients at Various R/L Ratios and S/L=0.2
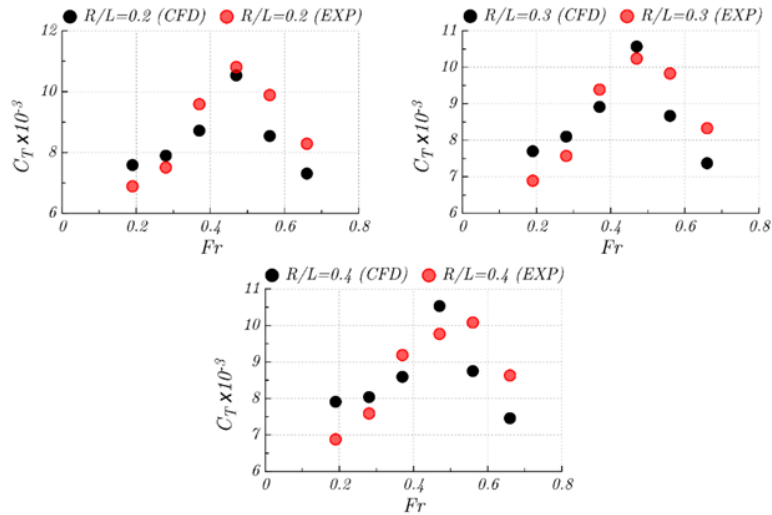
Fig. 8. Total Resistance Coefficients at Various R/L ratios and
S/L=0.4

These characteristics are merely related to its intrinsic nonlinearities' phenomena appear through her pressure and viscous resistances coefficients as comprehensively discussed in Sub-section 3.1 and 3.2. This is the reason why the catamaran resistance performance cannot be merely predicted with sufficient reliability when severe nonlinearities in the ensuing hydrodynamic behaviour between two demi-hulls existed. The theoretical approaches may be failed in the description of the phenomena, and don't possess sufficient forecasting capability, in quantitative aspects, qualitative ones and often in both. Therefore, some preliminary experimental model tests at towing-tank are accordingly undertaken for the various configurations of the symmetrical and the staggered catamaran models as summarized in Table 2.

The goodness of the comparison of computational simulation with the experimental data for the total ship's resistance coefficients stand as an initial validation of the CFD modelling (see Table 6, Table 7 and Table 8). This means that the computational simulations have successfully captured such nonlinearities with the acceptable results validation both in a qualitative and quantitative sense, where the average of the discrepancy percentage is below 10%. The stage has now been reached where the current CFD setting can be confidently used to assess the pressure and viscous resistances of the symmetrical and staggered catamaran in a given different Froude numbers.

Table 6
Validation of Total Resistance Coefficients of Symmetrical Catamaran

S/L = 0.2 C_T (x10^{-3})			S/L = 0.3 C_T (x10^{-3})			S/L = 0.4 C_T (x10^{-3})		
CFD	EXP.	%Error	CFD	EXP.	%Error	CFD	EXP.	%Error
7.3744	7.29	-1.16	7.2964	6.83	-6.83	7.3691	6.77	-8.85
8.4278	8.88	5.09	8.0492	8.20	1.84	7.7303	7.49	-3.21
9.2212	9.30	0.85	8.3227	8.55	2.66	7.9065	8.53	7.31
11.8035	11.93	1.06	10.9023	11.85	8.00	10.5459	11.22	6.01
9.4650	10.80	12.36	8.7519	9.94	11.95	8.5966	9.66	11.01
7.8663	8.56	8.10	7.3393	8.20	10.50	7.4161	8.10	8.44

Table 7
Total Resistance Coefficients of Staggered Catamaran at Various R/L Ratios (S/L=0.2)

S/L	R/L	Fr	C_T (x10^{-3}) CFD	C_T (x10^{-3}) EXP.	%Error
		0.19	7.5501	7.3500	-2.72
		0.28	8.0392	8.1300	1.12
	0.2	0.37	8.5713	9.2900	7.74
		0.47	11.4630	11.7300	2.28
		0.56	9.2567	10.7700	14.05
		0.66	7.7112	8.9100	13.45
		0.19	7.7137	7.6900	-0.31
		0.28	8.3170	8.8600	6.13
0.2	0.3	0.37	8.2891	8.9200	7.07
		0.47	11.1316	10.8600	-2.50
		0.56	9.1320	10.6700	14.41
		0.66	7.7430	9.0700	14.63
		0.19	7.6749	7.9100	2.97
		0.28	8.9767	9.6000	6.49
	0.4	0.37	8.2032	9.4900	13.56
		0.47	10.7883	9.9100	-8.86
		0.56	9.0440	10.5900	14.60
		0.66	7.7806	9.1820	15.26

Table 8
Total Resistance Coefficients of Staggered Catamaran at Various *R/L* Ratios (*S/L* = 0.4)

S/L	R/L	Fr	C_T (x10^{-3}) CFD	C_T (x10^{-3}) EXP.	%Error
		0.19	7.5898	6.8900	-10.16
		0.28	7.9000	7.5100	-5.19
	0.2	0.37	8.7200	9.5900	9.07
		0.47	10.5343	10.8100	2.55
		0.56	8.5455	9.8900	13.59
		0.66	7.3065	8.2900	11.86
		0.19	7.7025	6.8900	-11.79
		0.28	8.1004	8.5700	5.48
0.4	0.3	0.37	8.9147	9.3900	5.06
		0.47	10.5661	10.2400	-3.18
		0.56	8.6654	9.8300	11.85
		0.66	7.3726	8.3300	11.49
		0.19	7.9100	6.8800	-14.97
		0.28	8.0405	7.5900	-5.94
	0.4	0.37	8.5912	9.1900	6.52
		0.47	10.5315	9.7700	-7.79
		0.56	8.7508	10.0800	13.19
		0.66	7.4582	8.6300	13.58

4.1 Effect of Lateral Separation on Pressure and Viscous Resistances of Symmetrical Catamaran

The characteristics of pressure and viscous resistance of the symmetrical catamaran are displayed in Figure 9. In general, the subsequent increase of the Froude numbers form Fr=0.19 up to Fr=0.37, the results are proportional with C_P and C_V. However, this is inversely proportional with the viscous coefficient values. The results show that the lateral separation ratio with S/L=0.2 has highest

value of C_P; and we obtain that the viscous coefficients can be considered negligible small effects regardless of the S/L ratios.
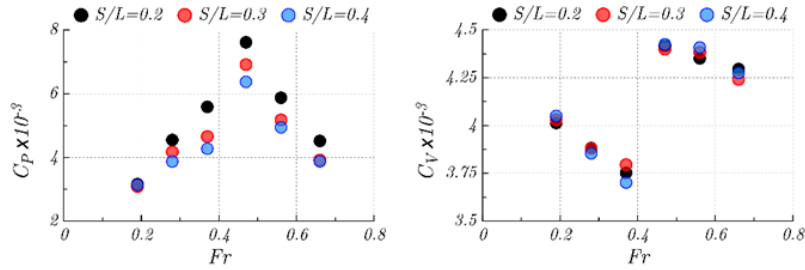
Fig. 9. Pressure and Viscous Coefficients of Symmetrical Catamaran with Different S/L Ratios

Referring to Table 9, Table 10, and Table 11, it is worth to note that the most unfavourable interference factor occurs at Fr=0.47, which is quantified via the sufficient increase of the C_P and C_V values. It should be noted that the significant increase of C_P takes place as the increase of Fr from 0.37 to 0.47 by 36%, 48% and 49% at S/L ratios 0.2, 0.3 and 0.4, respectively; meanwhile, the value of C_V increases by 18%, 16% and 20% at the S/L ratios 0.2, 0.3 and 0.4, respectively. In addition to the effect of the S/L ratios, the pressure coefficient has reduced by 9% and 8% as subsequently changing of the lateral separation ratio from 0.2 to 0.3 and 0.3 to 0.4, respectively; whilst the viscous resistance coefficient behaves nonlinearly where the value of C_V reduces by 0.4% and inversely increases by 0.6% for the aforementioned S/L ratios alterations. Furthermore, the values of C_P and C_V gradually decrease with the range of the Froude number $0.56 \leq Fr \leq 0.66$. Similar to what was reported by Sulistyawati *et al.*, [29], this may occur due to the favourable hydrodynamic factors which lead to reduce the pressure and viscous resistance coefficients as well as the total ship's resistance coefficient.

Table 9
C_P and C_V values at S/L=0.2

S/L	R/L	Fr	C_P ($\times 10^{-3}$)	C_V ($\times 10^{-3}$)
		0.19	3.1652	4.0131
		0.28	4.5495	3.8816
0.2	0	0.37	5.5873	3.7525
		0.47	7.6166	4.4158
		0.56	5.8731	4.3513
		0.66	4.5200	4.2955

Table 10
C_P and C_V values at S/L = 0.3

S/L	R/L	Fr	C_P ($\times 10^{-3}$)	C_V ($\times 10^{-3}$)
		0.19	3.0892	4.0300
		0.28	4.1727	3.8789
0.3	0	0.37	4.6549	3.7951
		0.47	6.9157	4.3995
		0.56	5.1795	4.3831
		0.66	3.9191	4.2411

Table 11
C_P and C_V values at S/L=0.4

S/L	R/L	Fr	C_P ($\times 10^{-3}$)	C_V ($\times 10^{-3}$)
		0.19	3.1389	4.0502
		0.28	3.8714	3.8545
0.4	0	0.37	4.2727	3.7019
		0.47	6.3734	4.4242
		0.56	4.9440	4.4086
		0.66	3.8764	4.2751

Furthermore, the explanation of CFD results have been put forward to explain the hydrodynamic characteristics of the pressure and viscous resistances at the various S/L ratios as depicted in Figures 10 and 11. The pressure resistance is proportional correspondingly to the forward velocities. This

can be explained by the fact that the subsequent increase of the pressure resistance occurs due to presence of the high-pressure gradients (red colour) that appear at the ship's bow regions as seen in Figures 10(a)-10(f).

(a) S/L = 0.2, R/L = 0, Fr = 0.19

(b) S/L = 0.2, R/L = 0, Fr = 0.28

(c) S/L = 0.2, R/L = 0, Fr = 0.37

(d) S/L = 0.2, R/L = 0, Fr = 0.47

(e) S/L = 0.2, R/L = 0, Fr = 0.56

(f) S/L = 0.2, R/L = 0, Fr = 0.66
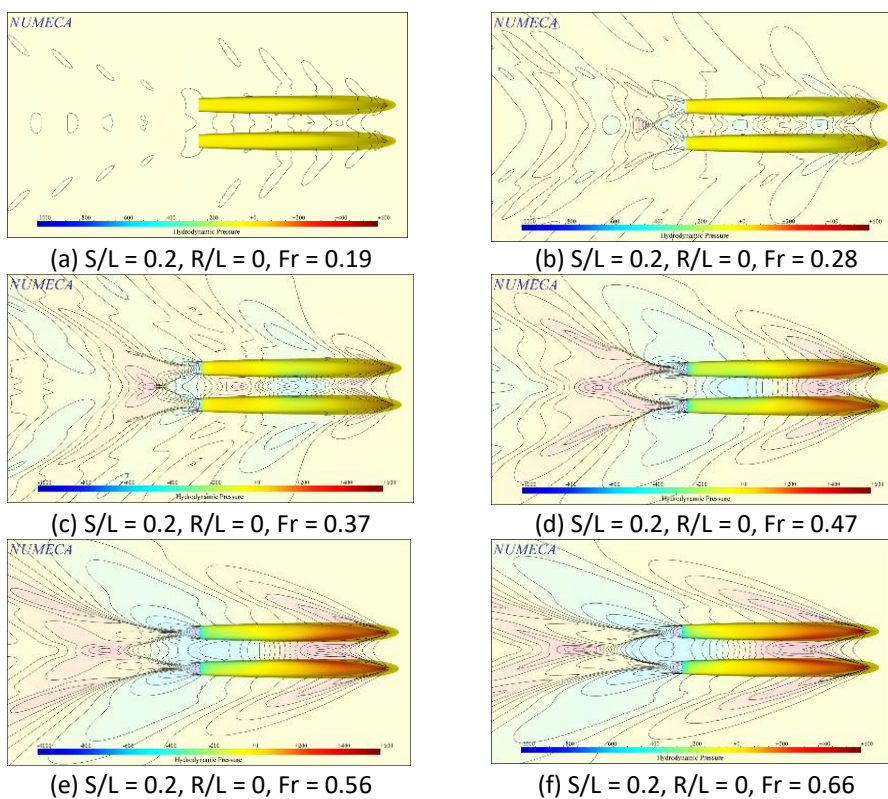
Fig. 10. Hydrodynamics Pressure at Various Froude Numbers

(a) S/L = 0.2, R/L = 0, Fr = 0.19

(b) S/L = 0.2, R/L = 0, Fr = 0.28

(c) S/L = 0.2, R/L = 0, Fr = 0.37

(d) S/L = 0.2, R/L = 0, Fr = 0.47

(e) S/L = 0.2, R/L = 0, Fr = 0.56

(f) S/L = 0.2, R/L = 0, Fr = 0.66
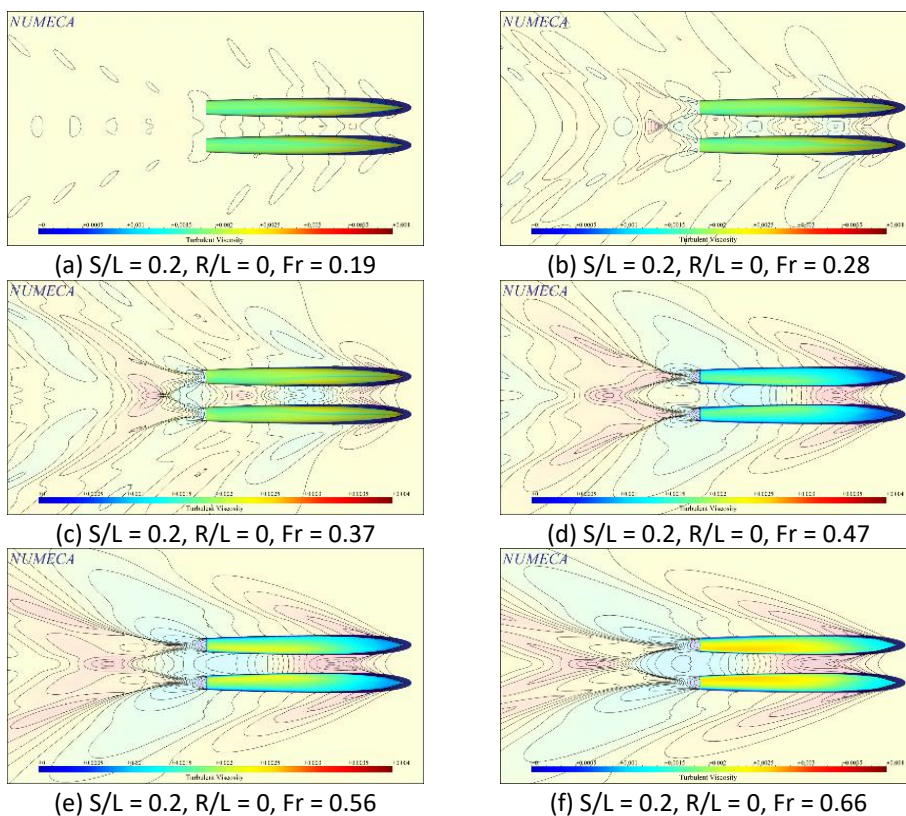
Fig. 11. Turbulent Viscosity at Various Froude Numbers

It should be noted here that the lowest separation ratio (S/L=0.2) appears to have a highest-pressure coefficient with respect to the Froude numbers, especially at Fr=0.47 (see Figure 12).

S/L = 0.2, R/L = 0, Fr = 0.47   S/L = 0.3, R/L = 0, Fr = 0.47
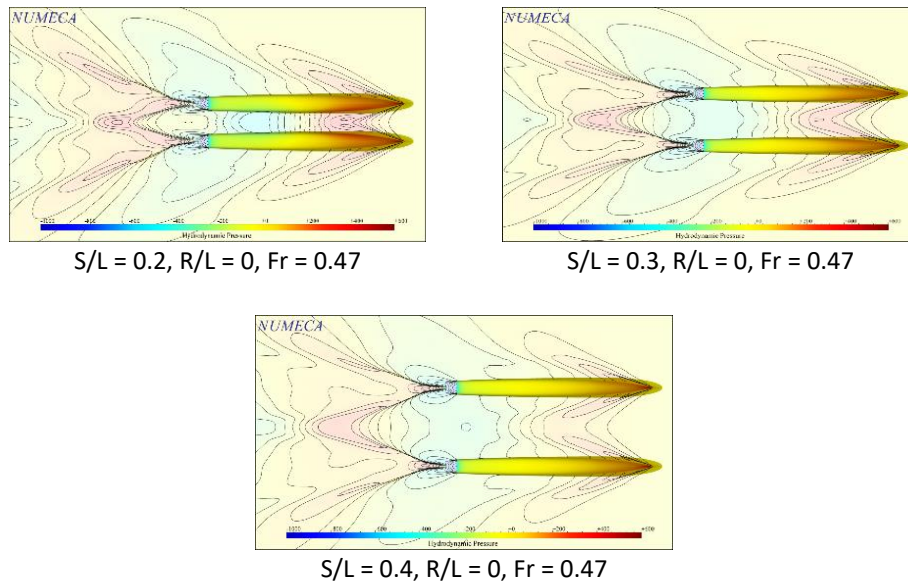
S/L = 0.4, R/L = 0, Fr = 0.47
Fig. 12. Hydrodynamic Pressure at Various S/L Ratios

This occurred mostly due to the stronger contribution of the wave interference between the two demi-hulls. Moreover, this could be also the basic reason of the augmented pressure induced by the wave-making resistance particularly in between the narrower lateral separation as noted by Papanikolaou and Dafnias [29], where Fr around 0.45 was identified as an unfavourable Froude number for the catamaran resistance. In addition, Stefano *et al.*, [30] stated that the maximum value for the interference has taken place for the Froude numbers around 0.50; this underlines the reason why the catamaran seemed to have the unfavourable influence on the total resistance coefficient. But it should be said that the interference factor is then moderately diminished upon increasing S/L ratios as visually displayed in Figures 10(e) and 10(f).

The computational results show that the viscous resistance coefficient tends to decrease with the range of Froude numbers $0.19 \leq Fr \leq 0.37$; and rapidly increase at Fr=0.47. The further increase of the Froude numbers leads to gradually reduce the value of C_V. The characteristics of the viscous resistance of the symmetrical catamaran model is presented in Figure 11. The existence of the higher turbulent viscosity (yellow colour) at low speed extends over the entire hull surfaces of the catamaran as seen in Figures 11(a)-11(c). However, the viscous resistance coefficient remains in existence and imposes nearby the inner hull surfaces of the catamaran as displayed in Figure 11(d). In addition, Figure 11(f) show that the presence of the stronger flow separation in the aft body causes the value of C_V gradually reduces. This can be explained by the fact that this favourable interference corresponded to conditions where the wave systems tend to coincide in cancelling each other out at the inner region. In other words, this negligible or favourable interference region clearly corresponds to the local minimum in the resistance coefficient as reported by Stefano *et al.*, [30]. Similar to was noted above, the flow around catamaran with S/L=0.2 produces higher wave interference factors as compared to the ratio of S/L=0.3 and 0.4 (see Figure 13), which is proportional to the magnitude of the viscous resistance Setyawan *et al.*, [31]. Merely, it can be concluded that the subsequent increase of lateral separation ratio will affect the viscous and pressure coefficients.

S/L = 0.2, R/L = 0, Fr = 0.47   S/L = 0.3, R/L = 0, Fr = 0.47
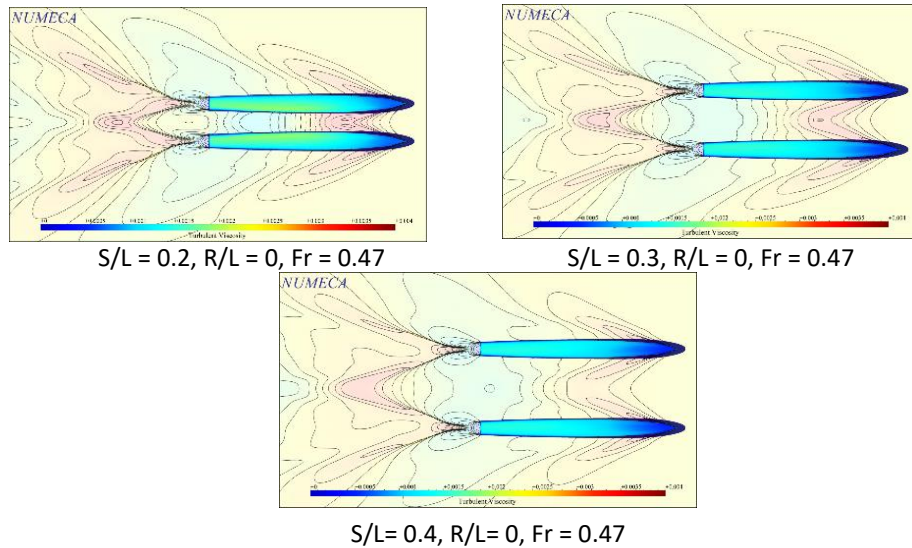
S/L= 0.4, R/L= 0, Fr = 0.47
Fig. 13. Turbulent Viscosity at Various S/L Ratios

4.2 Effect of Longitudinal Separation on Pressure and Viscous Resistances of Symmetrical Catamaran

Leaving the arguments about an impracticality in the real construction of the staggered catamaran configuration, this computational investigation provides insight into a better understanding of the hydrodynamic interactions via quantifying the pressure and viscous resistances coefficients as shown in Figures 14 and 15.
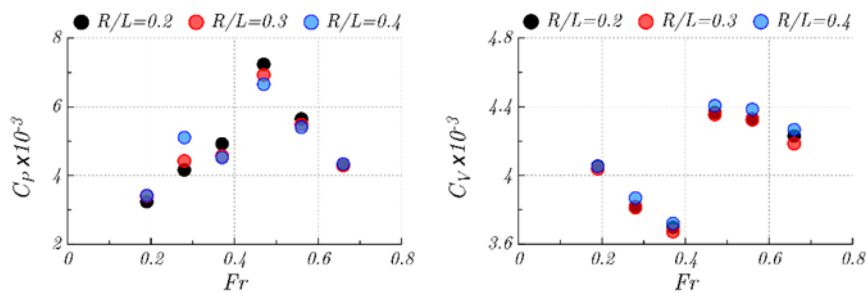
Fig. 14. Pressure (Top-Left) and Viscous (Top-Right) Resistances
Coefficients of Catamaran at Various R/L Ratios (S/L=0.2)
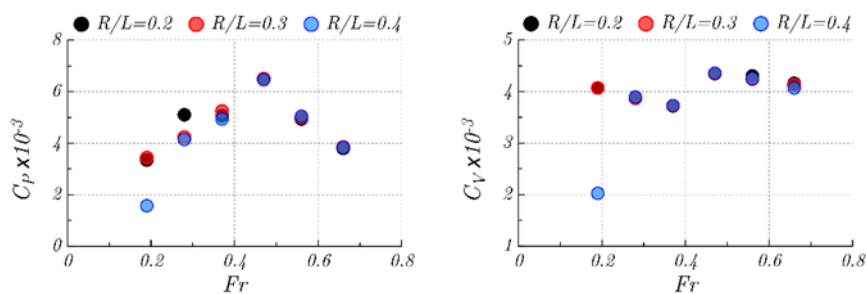
Fig. 15. Pressure (Top-Left), Viscous (Top-Right) and Resistances
Coefficients of Catamaran at Various R/L Ratios (S/L= 0.4)

Here, two different cases of the lateral separation ratio S/L=0.2 and 0.4 have been considered to analyses the effect of various longitudinal staggered ratios at Fr=0.47. The results reveal that S/L=0.2 produces higher viscous and pressure coefficients regardless of R/L ratios than the lateral separation ratio of 0.4. Besides, this demonstrates that the staggered catamaran with R/L=0.2 has the most

unfavourable interference effect both of S/L=0.2 and S/L=0.4 indicated with the higher resistance coefficients of C_P and C_V. The detailed data of the pressure and viscous resistances coefficients acting the staggered catamaran configurations are presented in Table 12 and 13.

Table 12
C_P and C_V at Various *R/L* Ratios (*S/L* =0.2)

S/L	R/L	Fr	C_P (x10⁻³)	C_V (x10⁻³)
		0.19	3.2405	4.0538
		0.28	4.1659	3.8185
	0.2	0.37	4.9258	3.6979
		0.47	7.2384	4.3658
		0.56	5.6489	4.3290
		0.66	4.2969	4.2299
		0.19	3.4105	4.0387
		0.28	4.4236	3.8127
0.2	0.3	0.37	4.5666	3.6726
		0.47	6.9307	4.3547
		0.56	5.4816	4.3243
		0.66	4.2940	4.1856
		0.19	3.4186	4.0543
		0.28	5.1083	3.8696
	0.4	0.37	4.5247	3.7212
		0.47	6.6595	4.4061
		0.56	5.4053	4.3853
		0.66	4.3365	4.2667

Table 13
C_P and C_V at Various *R/L* Ratios (*S/L* = 0.4)

S/L	R/L	Fr	C_P (x10⁻³)	C_V (x10⁻³)
		0.19	3.3452	4.0698
		0.28	5.1083	3.8696
	0.2	0.37	5.0682	3.7212
		0.47	6.4851	4.3512
		0.56	4.9414	4.3041
		0.66	3.8001	4.1594
		0.19	3.4352	4.0692
		0.28	4.2356	3.8708
0.4	0.3	0.37	5.2525	3.7236
		0.47	6.5029	4.3510
		0.56	5.0023	4.2452
		0.66	3.8490	4.1296
		0.19	1.5695	2.0251
		0.28	4.1457	3.8934
	0.4	0.37	4.9416	3.7263
		0.47	6.4629	4.3572
		0.56	5.0448	4.2496
		0.66	3.8403	4.0724

Comparing the results of the staggered catamaran with S/L=0.2, in general, the subsequent increase of the aforementioned longitudinal staggered ratios with S/L=0.4 is considered to have a relatively small effect corresponds to the pressure and viscous resistances coefficients. Merely, in what appears to be qualitatively similar trends with respect to the characteristics of the pressure

and viscous resistances coefficients of the symmetrical catamaran configurations. This seemingly reasonable finding can be explained by observing the hydrodynamic characteristics as well-noted in Sub-section 3.1. In case of S/L=0.2 (see Figure 16), it is noteworthy that the wave interferences on the staggered catamaran of R/L=0.2, 0.3 and 0.4 have led to be more unfavourable effects indicated with the significant percentage increments of C_P by 68%, 117% and 53%, respectively; whilst, the percentage of C_V increases by 7%, 10% and 9%, respectively, as compared to S/L=0.4 with similar R/L ratios (see Figure 17).

R/L = 0.2, Fr = 0.47

R/L = 0.3, Fr = 0.47

R/L = 0.4, Fr = 0.47

Fig. 16. Hydrodynamic Pressure at Various R/L Ratios (S/L=0.2)

R/L = 0.2, Fr = 0.47

R/L = 0.3, Fr = 0.47

R/L = 0.4, Fr = 0.47
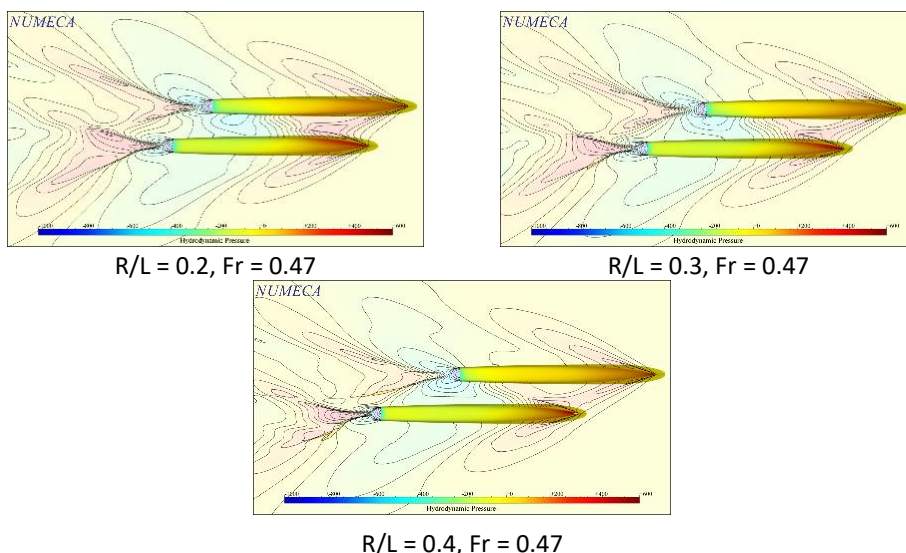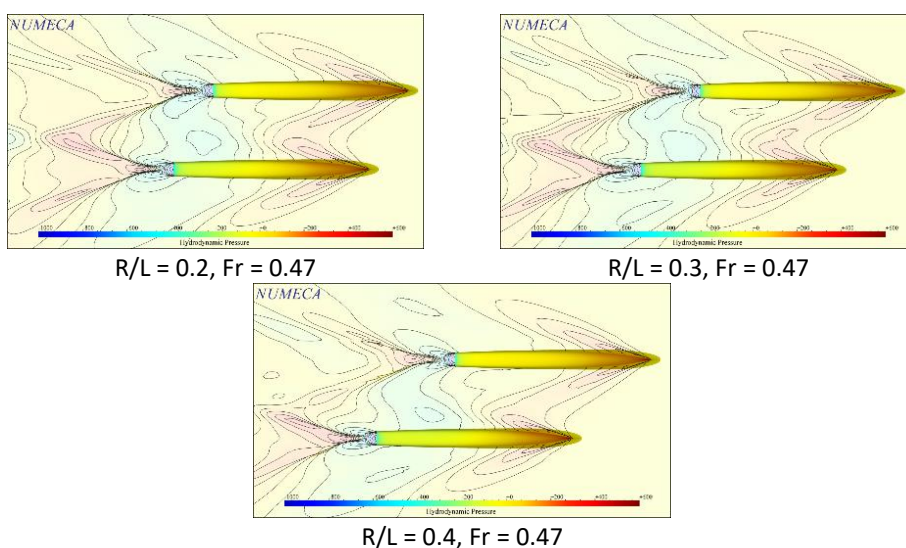
Fig. 17. Hydrodynamic Pressure at Various R/L Ratios (S/L=0.4)

The CFD visualizations explained that the wave crests close to the bow gradually are being reduced, which are proportional to the magnitude of the wave elevations in the inner regions displaying much weaker pressure gradients at the two demi hulls. This means that the existence of the wave crest (the higher wave amplitude) is prone to decrease or even disappear along the one inner-side of the demi hull upon increasing R/L ratios, which works to diminish the wave-making resistance. As compared with various longitudinal staggered ratios from R/L=0.2 to R/L=0.3 and R/L=0.3 to R/L=0.4, the results showed that an insignificant effect of viscous coefficient with 0.25% and 1.2% of discrepancy percentage. It was pointed out here that the catamaran with R/L=0.4 has

been generate the highest value of viscous coefficient as compared to the R/L=0.2 and R/L=0.3. This is due to higher turbulent viscosity (yellow colour) region appears at the surface of the hull as displayed in Figures 18 and 19.

R/L = 0.2, Fr = 0.47   R/L = 0.3, Fr = 0.47

R/L = 0.4, Fr = 0.47

Fig. 18. Hydrodynamic Pressure at Various R/L Ratios (S/L=0.2)

R/L = 0.2, Fr = 0.47   R/L = 0.3, Fr = 0.47

R/L = 0.4, Fr = 0.47
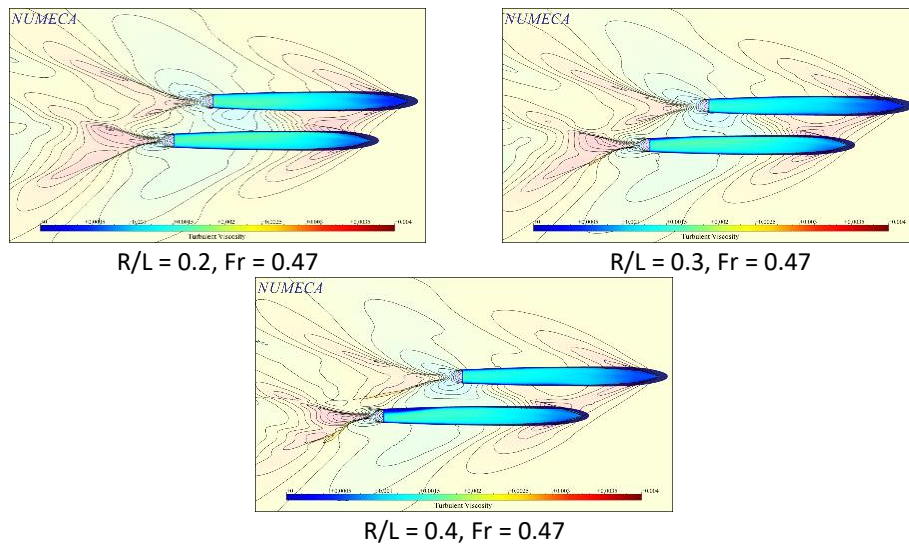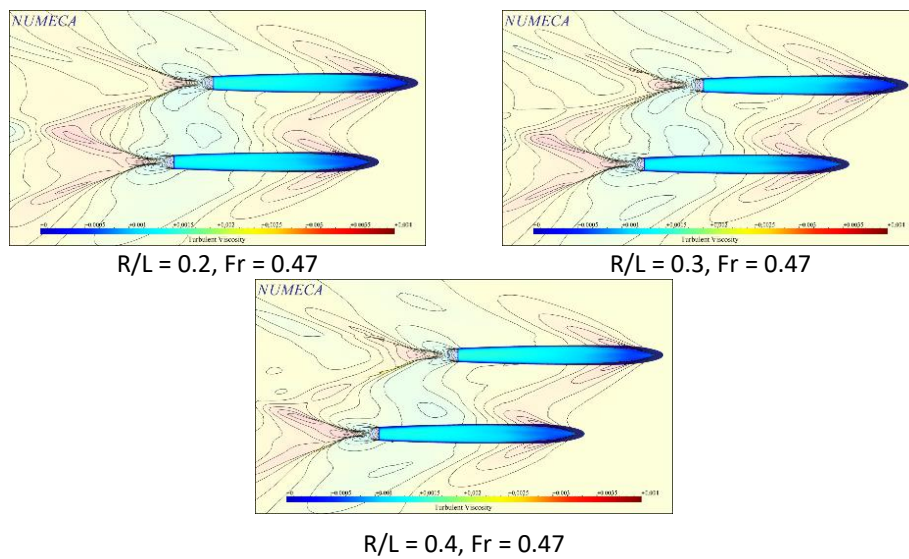
Fig. 19. Hydrodynamic Pressure at Various R/L Ratios (S/L=0.4)

It should be simply noted that the transverse waves from the bow travels aft of the staggered catamaran with larger R/L ratios lead to increase the viscous resistance coefficients. Hence, this can be concluded that the increasing its longitudinal staggered ratio will be an ideal solution to provide a beneficial reduction in its pressure coefficient, but it is inversely to the viscous coefficient.

5. Conclusion

The computational investigation into the viscous and pressure resistances of the symmetrical and staggered catamaran configurations provide an insight of these characteristics with respects to a wide range of Froude number involving a complex hydrodynamics phenomenon between two demi hull. The computation results are concluded as follows:

i. In general, the increase of Froude number from 0.19 up to 0.66 produces the highest viscous and pressure coefficient at Fr=0.47 regardless of the symmetrical and staggered catamaran models.

ii. The value of the pressure resistance coefficient at the various lateral separation ratios of the symmetrical catamaran has more dominant effect into the total ship's resistance. This occurred due to presence of the higher-pressure gradients at the ship's bow regions; whilst the viscous resistance can be considered negligible small effects.

iii. Comparing the results of R/L ratios on the staggered catamaran model, the subsequent increase of the longitudinal separation ratio has led to produce larger viscous coefficient; and inversely, the pressure resistance co-efficient has taken place dominantly.

Acknowledgement

References

[1] Insel, Mustafa. "An investigation into the resistance components of high speed displacement catamarans." PhD diss., University of Southampton, 1990.

[2] Seif, Mohammad Saeed, and E. Amini. "Performance comparision between planing monohull and catamaran at high froude numbers." (2004): 435-441.

[3] Peng, Hongxuan. "Numerical computation of multi-hull ship resistance and motion." (2001).

[4] Utama, Ketut Aria Pria, Andi Jamaluddin, and W. D. Aryawan. "EXPERIMENTAL INVESTIGATION INTO THE DRAG INTERFERENCE OF SYMMETRICAL AND ASYMMETRICAL STAGGERED AND UNSTAGGERED CATAMARANS." *Journal of Ocean Technology* 7, no. 1 (2012).

[5] Molland, A. F., J. F. Wellicome, and P. R. Couser. "Resistance experiments on a systematic series of high speed displacement catamaran forms: variation of length-displacement ratio and breadth-draught ratio." (1994).

[6] Molland, A. F., P. A. Wilson, and D. J. Taunton. "Resistance experiments on a systematic series of high speed displacement monohull and catamaran forms in shallow water." (2003). https://doi.org/10.3940/rina.ijme.2004.a2.3604

[7] Broglia, Riccardo, Boris Jacob, Stefano Zaghi, Frederick Stern, and Angelo Olivieri. "Experimental investigation of interference effects for high-speed catamarans." *Ocean Engineering* 76 (2014): 75-85. https://doi.org/10.1016/j.oceaneng.2013.12.003

[8] Zaghi, Stefano, Riccardo Broglia, and Andrea Di Mascio. "Experimental and numerical investigations on fast catamarans interference effects." *Journal of Hydrodynamics, Ser. B* 22, no. 5 (2010): 528-533. https://doi.org/10.1016/S1001-6058(09)60250-X

[9] Broglia, Riccardo, Stefano Zaghi, and Andrea Di Mascio. "Numerical simulation of interference effects for a high-speed catamaran." *Journal of marine science and technology* 16 (2011): 254-269. https://doi.org/10.1007/s00773-011-0132-3

[10] Haase, Max, Jonathan Binns, Giles Thomas, and Neil Bose. "Resistance Prediction of Mediumspeed Catamarans Using Free-surface Viscous Flow Simulations." In *15th Numerical Towing Tank Symposium*. 2012.

[11] He, Wei, Teresa Castiglione, Manivannan Kandasamy, and Frederick Stern. "Numerical analysis of the interference effects on resistance, sinkage and trim of a fast catamaran." *Journal of marine science and technology* 20 (2015): 292-308. https://doi.org/10.1007/s00773-014-0283-0

[12] Zaghi, Stefano, Riccardo Broglia, and Andrea Di Mascio. "Analysis of the interference effects for high-speed catamarans by model tests and numerical simulations." *Ocean Engineering* 38, no. 17-18 (2011): 2110-2122. https://doi.org/10.1016/j.oceaneng.2011.09.037

[13] Sadeghi, Mohamad, and Ahmad Hajivand. "Investigation the effect of canted rudder on the roll damping of a twin-rudder ship." *Applied Ocean Research* 103 (2020): 102324. https://doi.org/10.1016/j.apor.2020.102324

[14] Sadeghi, Mohamad, and Hamid Zeraatgar. "Investigation on the effect of anti-pitch fins for reducing the motion and acceleration of ships using computational fluid dynamics." *Ocean Engineering* 267 (2023): 112965. https://doi.org/10.1016/j.oceaneng.2022.112965

[15] Fitriadhy, A., P. S. Lim, and A. Jamaluddin. "CFD Investigation on total resistance coefficient of symmetrical and staggered catamaran configurations through quantifying existence of an interference factor." In *International Conference on Ships and Offshore Structures. Hamburg, Germany*. 2016.

[16] Adam, N. Amira, A. Fitriadhy, C. J. Quah, and T. Haryanto. "Computational analysis on B-series propeller performance in open water." *Marine Systems & Ocean Technology* 15, no. 4 (2020): 299-307. https://doi.org/10.1007/s40868-020-00087-z

[17] Fitriadhy, Ahmad, and Amira Adam. "CFD analysis on vertical motion of a full-scale floating jetty." *Journal of Sustainability Science and Management* 15, no. 6 (2020): 100-110. https://doi.org/10.46754/jssm.2020.08.009

[18] Fitriadhy, Ahmad, Nur Adlina Aldin, and Nurul Aqilah Mansor. "CFD analysis on course stability of a towed ship incorporated with symmetrical bridle towline." *CFD Letters* 11, no. 12 (2019): 88-98.

[19] Fitriadhy, Ahmad, Intan Nur Nabila, Christina Bangi Grosnin, Faisal Mahmuddin, and Suandar Baso. "Computational Investigation into Prediction of Lift Force and Resistance of a Hydrofoil Ship." *CFD Letters* 14, no. 4 (2022): 51-66. https://doi.org/10.37934/cfdl.14.4.5166

[20] Menter, Florian R. "Influence of freestream values on k-omega turbulence model predictions." *AIAA journal* 30, no. 6 (1992): 1657-1659. https://doi.org/10.2514/3.11115

[21] Menter, Florian R. "Performance of popular turbulence model for attached and separated adverse pressure gradient flows." *AIAA journal* 30, no. 8 (1992): 2066-2072. https://doi.org/10.2514/3.11180

[22] Menter, Florianr. "Zonal two equation kw turbulence models for aerodynamic flows." In *23rd fluid dynamics, plasmadynamics, and lasers conference*, p. 2906. 1993. https://doi.org/10.2514/6.1993-2906

[23] Menter, Florian R. "Two-equation eddy-viscosity turbulence models for engineering applications." *AIAA journal* 32, no. 8 (1994): 1598-1605. https://doi.org/10.2514/3.12149

[24] Spalart, Philippe, and Steven Allmaras. "A one-equation turbulence model for aerodynamic flows." In *30th aerospace sciences meeting and exhibit*, p. 439. 1992. https://doi.org/10.2514/6.1992-439

[25] Baldwin, Barrett, and Timothy Barth. "A one-equation turbulence transport model for high Reynolds number wall-bounded flows." In *29th aerospace sciences meeting*, p. 610. 1991. https://doi.org/10.2514/6.1991-610

[26] Menter, Florian, and Christopher Rumsey. "Assessment of two-equation turbulence models for transonic flows." In *Fluid Dynamics Conference*, p. 2343. 1994. https://doi.org/10.2514/6.1994-2343

[27] Manual, N.U., FINE™/Marine v3.1. Flow Integrated Environment for Marine Hydrodynamics. Documentation v3.1a, NUMECA International, 2013: p. 187-189.

[28] Kim, Dong Jin, Sun Young Kim, Young Jun You, Key Pyo Rhee, Seong Hwan Kim, and Yeon Gyu Kim. "Design of high-speed planing hulls for the improvement of resistance and seakeeping performance." *International Journal of Naval Architecture and Ocean Engineering* 5, no. 1 (2013): 161-177. https://doi.org/10.2478/IJNAOE-2013-0124

[29] Papanikolaou, A., and N. Dafnias. "Hydrodynamic optimization and design of a fast displacement Catamaran Ferry." In *Proceeding of 6th international marine design conference, IMDC*, vol. 97. 1997.

[30] Zaghi, Stefano, Riccardo Broglia, and Andrea Di Mascio. "Analysis of the interference effects for high-speed catamarans by model tests and numerical simulations." *Ocean Engineering* 38, no. 17-18 (2011): 2110-2122. https://doi.org/10.1016/j.oceaneng.2011.09.037

[31] Setyawan, D., I. KAP Utama, Murdijanto Murdijanto, A. Sugiarso, and A. Jamaluddin. "Development of catamaran fishing vessel." *IPTEK the journal for technology and science* 21, no. 4 (2010). https://doi.org/10.12962/j20882033.v21i4.90